

“Urban Respiration” Revealed by Atmospheric O₂ Measurements in an Industrial Metropolis

Xiaoyue Liu, Jianping Huang,* Li Wang, Xinbo Lian, Changyu Li, Lei Ding, Yun Wei, Siyu Chen, Yongqi Wang, Shixue Li, and Jinsen Shi



Cite This: *Environ. Sci. Technol.* 2023, 57, 2286–2296



Read Online

ACCESS |

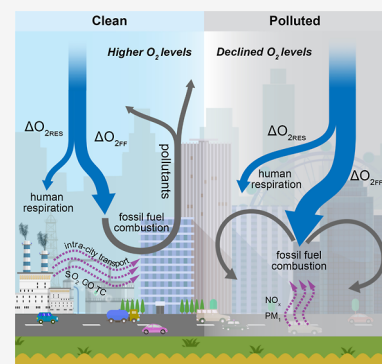
Metrics & More

Article Recommendations

Supporting Information

ABSTRACT: Urban regions, which “inhale” O₂ from the air and “exhale” CO₂ and atmospheric pollutants, including harmful gases and fine particles, are the largest sinks of atmospheric O₂, yet long-term O₂ measurements in urban regions are currently lacking. In this study, we report continuous measurements of atmospheric O₂ in downtown Lanzhou, an industrial metropolis in northwestern China. We found declines in atmospheric O₂ associated with deteriorated air quality and robust anticorrelations between O₂ and gaseous oxides. By combining O₂ and pollutants measurements with a Lagrangian atmospheric transport model, we quantitatively break down “urban respiration” (ΔO_{2URB}) into human respiration (ΔO_{2RES}) and fossil fuel combustion (ΔO_{2FF}). We found increased ΔO_{2FF} contribution (from 66.92% to 72.50%) and decreased ΔO_{2RES} contribution (from 33.08 to 27.50%) as O₂ declines and pollutants accumulate. Further attribution of ΔO_{2FF} reveals intracity transport of atmospheric pollutants from industrial sectors and suggests transportation sectors as the major O₂ sink in downtown Lanzhou. The varying relationships between O₂ and pollutants under different conditions unfold the dynamics of urban respiration and provide insights into the O₂ and energy consumption, pollutant emission, and intracity atmospheric transport processes.

KEYWORDS: urban O₂ measurements, air pollution, urban habitability, anthropogenic impact, vehicle pollutants



INTRODUCTION

Urban regions, with their large and dense populations, only account for 2% of global lands, but are home to more than 56% of the global population¹ and responsible for 70% of global fossil-fuel combustion.² In recent decades, as growing population streams into cities, urban regions have faced serious challenges regarding climate change adaptation and mitigation. Rapid urban expansion and the related land-use change have left a series of urban environmental issues including record-breaking urban heatwaves,³ extreme floods and droughts that overwhelm the undermaintained public infrastructures,⁴ rising levels of air pollution,^{5–7} and the emerging disturbed O₂ balance in urban regions.⁸

As a necessity for the survival of almost all living organisms on Earth, atmospheric oxygen (O₂) is one of the most critical gases in the atmosphere.^{9–11} However, continuous O₂ observations at ppm resolution are quite sparse since detecting minor O₂ variations against a large natural background is quite challenging.¹² Only a few organizations have conducted long-term atmospheric O₂ measurements, mostly in the natural background. The longest record of direct atmospheric O₂ measurements in the modern atmosphere shows a steady decline of approximately 4 ppm/yr since the late 1980s,¹³ which is generally attributable to fossil fuel combustion¹¹ and anthropogenic modifications to the land surface including deforestation.^{8,14} The aggressive urban expansion has not only

substantially boosted anthropogenic fossil fuel and O₂ consumption but also deprived the ecosystem of biological O₂ production and CO₂ fixation, breaking the atmospheric O₂ balance.^{15,16} A recent ice-core-based study attributed a decline in atmospheric O₂ since the Mid–Pleistocene transition (1.2–0.7 million years ago) to glacial weathering.¹⁷ Shi et al.¹⁸ and Chen et al.¹⁹ measured O₂ content over the Tibetan Plateau and implied reduced hypoxia risk on the Tibetan Plateau in a warming climate.

Urban regions “inhale” O₂ from the air and “exhale” CO₂ and atmospheric pollutants including harmful gases and fine particles. Thus, fossil fuel combustion and human respiration are two major anthropogenic O₂ sinks in the urban atmosphere. Approximately 55% of the world’s population occupies only 0.37% of the global land surface.^{20,21} In densely populated urban centers, human respiration could cause non-negligible perturbations in the observed O₂ and CO₂ flux and become potential sources of bias in the observation-constrained estimates since these studies ignored the influence of

Received: October 15, 2022

Revised: January 6, 2023

Accepted: January 6, 2023

Published: January 19, 2023



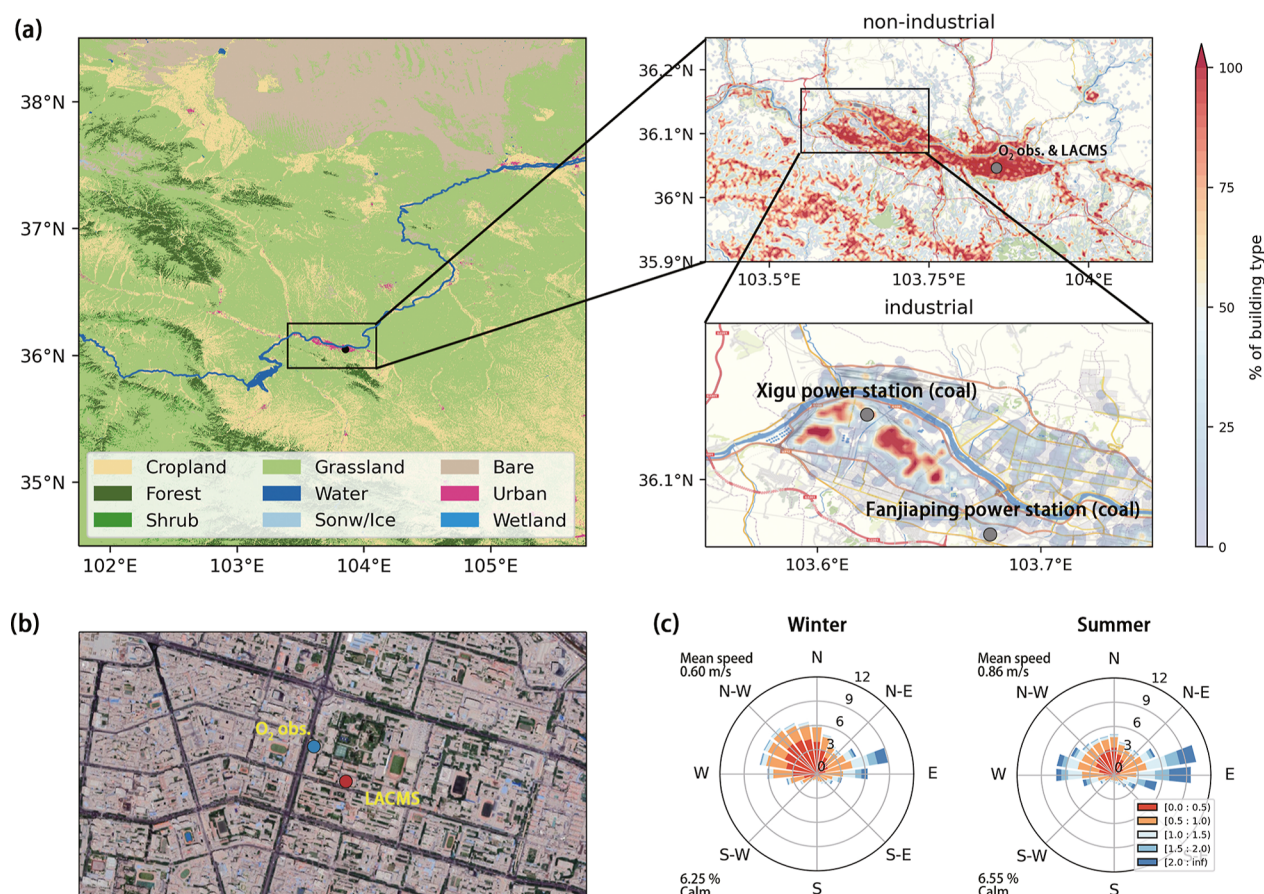


Figure 1. Geographic map and location of the observation station. (a) Map of Lanzhou Valley. The blue dot indicates the O₂ measurement site (LZU Oxygen Observatory) and the red dot indicates the LACMS. Shading indicates a population density with 0.01×0.01 grid spacing. (b) Satellite image around the measurement site (source: Google Earth). (c) Windrose plots at the LACMS in winter (December, January, and February) and summer (June, July, and August).

human respiration and solely attributed the observed CO₂ to fossil fuel combustion. However, only a few studies have touched upon this issue. Ciais et al.²² estimated that respiration-related CO₂ emission reaches 30% of the fossil fuel emission for Beijing and 20% for Chongqing based on agricultural statistics. Moriwaki and Kanda²³ assumed an emission rate of 8.87 CO₂ mg s⁻¹/person, and the estimated human respiration corresponds to 17–38% of total CO₂ flux in an area with a population density of 11,800 persons/km.² Another European study estimated 6.5–17% contribution to total CO₂ fluxes based on similar assumptions.²⁴ Cai et al.²⁵ estimated that human and livestock respiration can contribute to more than 5% of the carbon emission in almost half of the countries and argues that human and livestock respiration are equally crucial in the regional carbon budget. Flux measurements by Ishidoya et al.²⁶ quantitatively break down O₂ and CO₂ variation in urban Tokyo into combustions of liquid and gaseous fuel and estimated O₂ and CO₂ flux due to human respiration based on assumed oxidative ratio (OR) of 1.2 and population statistics. A more recent observation during the COVID-19 lockdown attributed reductions in CO₂ emission to decreased traffic volume and found a slight decrease in human respiration flux owing to decreased commuters.²⁷

The above-mentioned estimates usually rely on some prior knowledge, including assumed physical activity levels for humans, ORs, food consumption and supply, and so forth, while atmospheric observations in urban regions can also be

utilized to estimate the potential contribution from human respiration and fossil fuel combustion. Atmospheric pollutants, including CO, NO_x, SO₂, and so forth, could be introduced as novel constraints to quantify the anthropogenic O₂ fluxes. In previous studies, they serve as tracers for anthropogenic fossil fuel combustion due to their overlapping emission sources^{28–30} since they are irrelevant to biological processes. Therefore, if atmospheric O₂ and fossil-fuel-related pollutants can be simultaneously observed, the changing relationships between O₂ and pollutants could serve as practical constraints to distinguish fossil fuel combustion from respiration in an urban atmosphere without excessive reliance on prior knowledge. Understanding these processes helps to track and measure fossil fuel combustions, validate and calibrate emission inventories, assess the efficacy of climate mitigation efforts, and provide scientific guidance for urban planning organizations.

In this work, using multiple sources of in situ observations in the urban area of Lanzhou (Figure 1), we investigated the variation in atmospheric O₂ during June 2020 to August 2021 and attempted to break down the “urban respiration” (ΔO_{2URB}) into fossil fuel combustion (ΔO_{2FF}) and human respiration (ΔO_{2RES}) under different pollution levels. We also introduced a Lagrangian atmospheric transport model (STILT)^{31,32} and high-resolution urban land cover classification data sets³³ to discuss and contrast the impact of fossil fuel

combustion from industrial and nonindustrial sectors on ΔO_{2FF} .

DATA AND METHODS

Site Locations. Field measurements were conducted in Lanzhou, the capital city of Gansu Province in the semiarid region of northwestern China. Lanzhou, with a total population of >4 million, used to be one of the most polluted cities in the world, with an annual mean PM_{10} of $150 \mu\text{g}/\text{m}^3$, according to a WHO database.³⁴ The city is situated in a narrow river valley surrounded by mountains (Figure 1a). The inhibited atmospheric dispersion due to the unique topography, temperature inversion, low-boundary layer height, calm wind, and scant precipitation could frequently contribute to the steady accumulation of pollutants within the valley.³⁵

Urban Lanzhou can be divided into two regions according to their distinct urban functions, the downtown (nonindustrial) region and the industrial region. The industrial region (Xigu District) is located in the westernmost part of Lanzhou. As the largest petrochemical industrial base in western China, it had a large share of industrial production (50.29%) in its annual gross domestic product (GDP) in 2020.³⁶ Two coal-fired power stations were also located in the Xigu District. The downtown region (Chengguan District, Qilihe District, and Anning District) has the highest population density of up to 50 000 persons/ km^2 . The O_2 and pollutant measurements are performed in Chengguan District. The main land cover around the observation station is characterized by residential and business buildings (Figure 1b). The prevailing wind is northwest in winter and east in summer, with a high frequency of calm winds (>6.0%) throughout the year (Figure 1c). Measurements for this study were taken from July 2020 to August 2021. Since no COVID-19 lockdown was implemented in and around Lanzhou during observation, the impact of lockdown measures on observation can be ignored.

Measurements for Atmospheric Pollutants and O_2 . Particulate matter (PM) concentrations (TSP, PM_{10} , $PM_{2.5}$, and PM_1), gaseous pollutants (O_3 , SO_2 , NO, NO_2 , and CO), and meteorological parameters (temperature, relative humidity, air pressure, and wind) were observed at the Lanzhou Atmospheric Components Monitoring Superstation^{35,37} (LACMS; 36.05°N , 103.87°E , Figure 1b). See Section S1 for further details about measurement instruments and methods in the LACMS station.

Air samples for O_2 measurements were collected on a building roof at Lanzhou University (approximately 300 m away from the LACMS, see Figure 1b). Online O_2 measurements were carried out using a gas chromatograph (7890B, Agilent, USA) connected with a diaphragm at a constant flow rate to prevent thermal fractionation. The air samples were separated by a Molecular Sieve 5A Plot column and detected with a thermal conductivity detector (TCD).

The interference of the dilution effect may cause significant bias when O_2 levels are reported in volume fraction units (e.g., ppm). An increase or decrease in the total air volume due to the addition or removal of other gaseous species would disturb the observed O_2 mole fraction to an extent that cannot be ignored. Thus, the concentration of atmospheric O_2 is usually reported as the relative deviation in the molar O_2/N_2 ratio from a reference value

$$\Delta(O_2/N_2) = \left[\frac{(O_2/N_2)_{\text{sample}}}{(O_2/N_2)_{\text{reference}}} - 1 \right] \times 10^6$$

where the subscripts “sample” and “reference” denote the sample air and reference gas, respectively. $\Delta(O_2/N_2)$ is expressed in per meg, where 1 per meg = 1×10^{-6} . In this regard, the measured $\Delta(O_2/N_2)$ is only sensitive to the changes in O_2 and N_2 fluxes, while N_2 fluxes are typically several orders of magnitude smaller than O_2 fluxes.¹³ To compare O_2 and pollutant concentrations, we report the O_2 changes in ppm units. The ratio of 4.8 per meg/ppm is used to convert the observed $\Delta(O_2/N_2)$ to the O_2 anomaly relative to an arbitrary reference concentration (ΔO_2).

The fractionation effects can cause significant bias in O_2 measurements. Fractionation effects can influence the O_2/N_2 ratio inside the measurement instrument or even at the sample intake.³⁸ Compared with N_2 , O_2 has a higher molecular mass and tends to accumulate in areas with lower temperatures, higher pressure, and higher absolute humidity. Significant observation bias can occur when temperature, humidity, and pressure are not uniform within the instrument. In this work, we employed support vector regression to correct the original GC/TCD signals based on meteorological parameters measured during the same period (including temperature, mixing ratio, wind, pressure, etc.; see Section S2 for details). To verify our bias-corrected GC/TCD O_2 observation, a high-precision O_2 analyzer, Picarro G2207, based on the cavity ring-down spectroscopy³⁹ was also used for comparisons for 7 days. The high consistency between the two instruments guarantees the reliability and accuracy of the bias-corrected GC/TCD data. Comparative measurements between the gas chromatograph (7890B, Agilent, USA) and Picarro G2207 indicate a mean bias of -0.289 ± 2.908 ppm (Figure S2).

STILT Model. The stochastic time-inverted Lagrangian transport (STILT) model^{39,40} is an open-source Lagrangian particle dispersion model.^{31,32,40} It has been widely used to simulate the transport of pollution and greenhouse gases through the atmosphere. The STILT model releases an ensemble of air parcels from target observations (receptor) and tracks the movements of air parcels backward. The source region for the receptor is indicated by the value of footprint [$\text{ppm}/(\mu\text{mol m}^{-2} \text{ s}^{-1})$]. Higher values of footprints suggest higher contributions from the source region to the receptor. The STILT model was run from Jul. 2020 to Aug. 2021 using the hourly ERAS reanalysis data. To avoid reliance on prior emission estimation, we adopted the urban land cover data from the high-resolution World Urban Database and Access Portal Tools.³³ These data provide Local Climate Zone (LCZ) classifications at 120 m grid resolution, which shed light on localized infrastructure within the city. We convolved the simulated footprint with building type (urban buildings as well as the industrial and nonindustrial buildings within urban areas) fraction at $0.01^\circ \times 0.01^\circ$ resolution, defined as the footprint-normalized urban, industrial, and nonindustrial fraction [$P_{\text{urb}}(x,y)$, $P_{\text{ind}}(x,y)$, and $P_{\text{non-ind}}(x,y)$, respectively; see Section S3.1 for details]. We then sum $P(x,y)$ across the simulated space to obtain P , which serves as a metric to quantify the urban, industrial, and nonindustrial influences (P_{urb} , P_{ind} , and $P_{\text{non-ind}}$, respectively; $P_{\text{urb}} = P_{\text{ind}} + P_{\text{non-ind}}$) on the observation site.²⁹ Clean (polluted) days are defined as observations with $P_{\text{urb}} < 25\text{th percentile}$ ($P_{\text{urb}} > 75\text{th}$

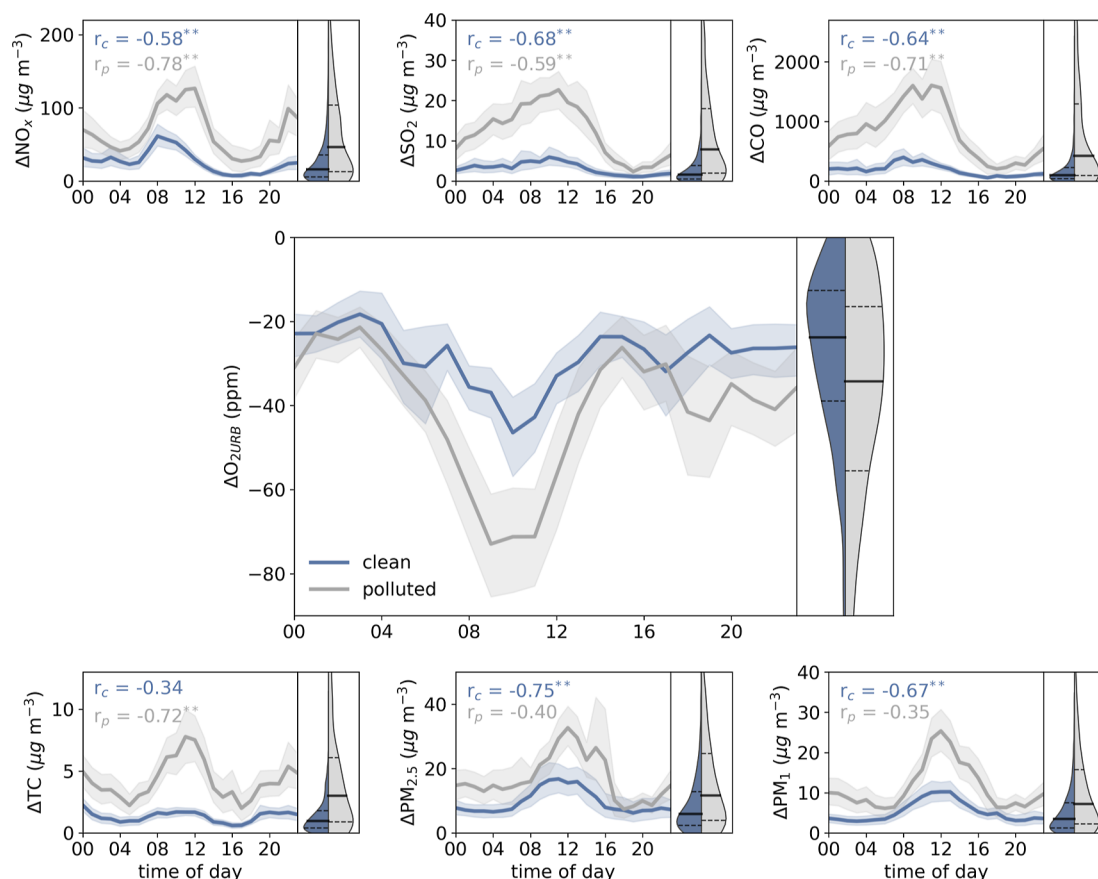
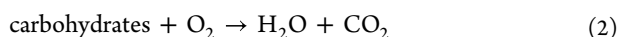
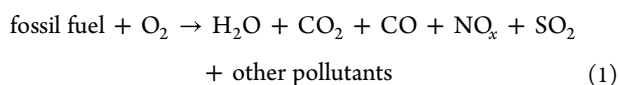


Figure 2. Averaged diurnal cycle of ΔPoll_i and $\Delta\text{O}_{2\text{URB}}$ for clean (blue) and polluted (grey) days, with shading representing a 95% confidence interval. A baseline concentration is subtracted from the original observation to highlight the anthropogenic signal. The right panel for each subplot is a violin plot that shows the probability distribution for observations under clean and polluted conditions. The Pearson correlation coefficients with the O_2 diurnal cycle on clean days (r_c) and polluted days (r_p) are shown in the left-top corner of each subplot. * and ** indicate statistical significance at the 95 and 99% confidence intervals, respectively.

percentile), indicating less (dominant) influence from urban sources.

Methods to Quantify “Urban Respiration”. To focus on the anthropogenic signals of O_2 and pollutants, a “baseline condition” that signifies the background influence should be established. Here, we derived baseline concentrations of O_2 using the 99th percentile within a 24 h window centered around each hourly data point (for pollutants, the 1st percentile was selected) and then applied a 24 h running average.³⁰ The baseline was then subtracted from the hourly concentration to determine the enhanced anthropogenic signals in O_2 and critical pollutants (denoted by $\Delta\text{O}_{2\text{URB}}$, ΔCO , ΔSO_2 , etc.), aiming to eliminate the contribution from background biological fluxes and highlight the anthropogenic influence (human respiration and fossil fuel combustion) in downtown Lanzhou (see Section S4.1 for details). Urban lands inhale O_2 and produce CO_2 and pollutants, including CO , NO_x , SO_2 , PM_{10} , and so forth. The following chemical reactions²⁸ could describe these oxidation processes



Equations 1 and 2 represent fossil fuel combustion and human respiration, respectively. The urban O_2 budget could be described as the following equation

$$\Delta\text{O}_{2\text{URB}} = \Delta\text{O}_{2\text{FF}} + \Delta\text{O}_{2\text{RES}} \quad (3)$$

where $\Delta\text{O}_{2\text{URB}} = \Delta\text{O}_2 - \Delta\text{O}_{2\text{baseline}}$.

According to the law of chemical mass balance, the O_2 consumption due to fossil fuel combustion ($\Delta\text{O}_{2\text{FF}}$) could be parametrized as the linear combination of fossil-fuel-related pollutants

$$\Delta\text{O}_{2\text{FF}} = -\sum_{i=0}^n k_i \times \Delta\text{Poll}_i \quad (4)$$

where n represents the number of pollutants introduced, k_i denotes the consumption coefficient of the i th pollutant, and Poll_i refers to the concentration of the i th pollutant.

To combine eqs 3 and 4, we have

$$\Delta\text{O}_{2\text{URB}} = -\sum_{i=0}^n k_i \times \Delta\text{Poll}_i + \Delta\text{O}_{2\text{RES}} \quad (5)$$

To solve eq 5, we bootstrapped $\Delta\text{O}_{2\text{URB}}$ and ΔPoll_i for 5000 times (each time with 30% samples). Then, non-negative least-square regression is applied to obtain 5,000 sets of bootstrap coefficients ($-k_i$) and intercepts ($-\Delta\text{O}_{2\text{RES}}$), and $\Delta\text{O}_{2\text{URB}}$ (<0) for each set is set to the absolute value ($-\Delta\text{O}_{2\text{URB}} > 0$). The averaged k_i and $\Delta\text{O}_{2\text{RES}}$ of the 5000 sets regression is obtained

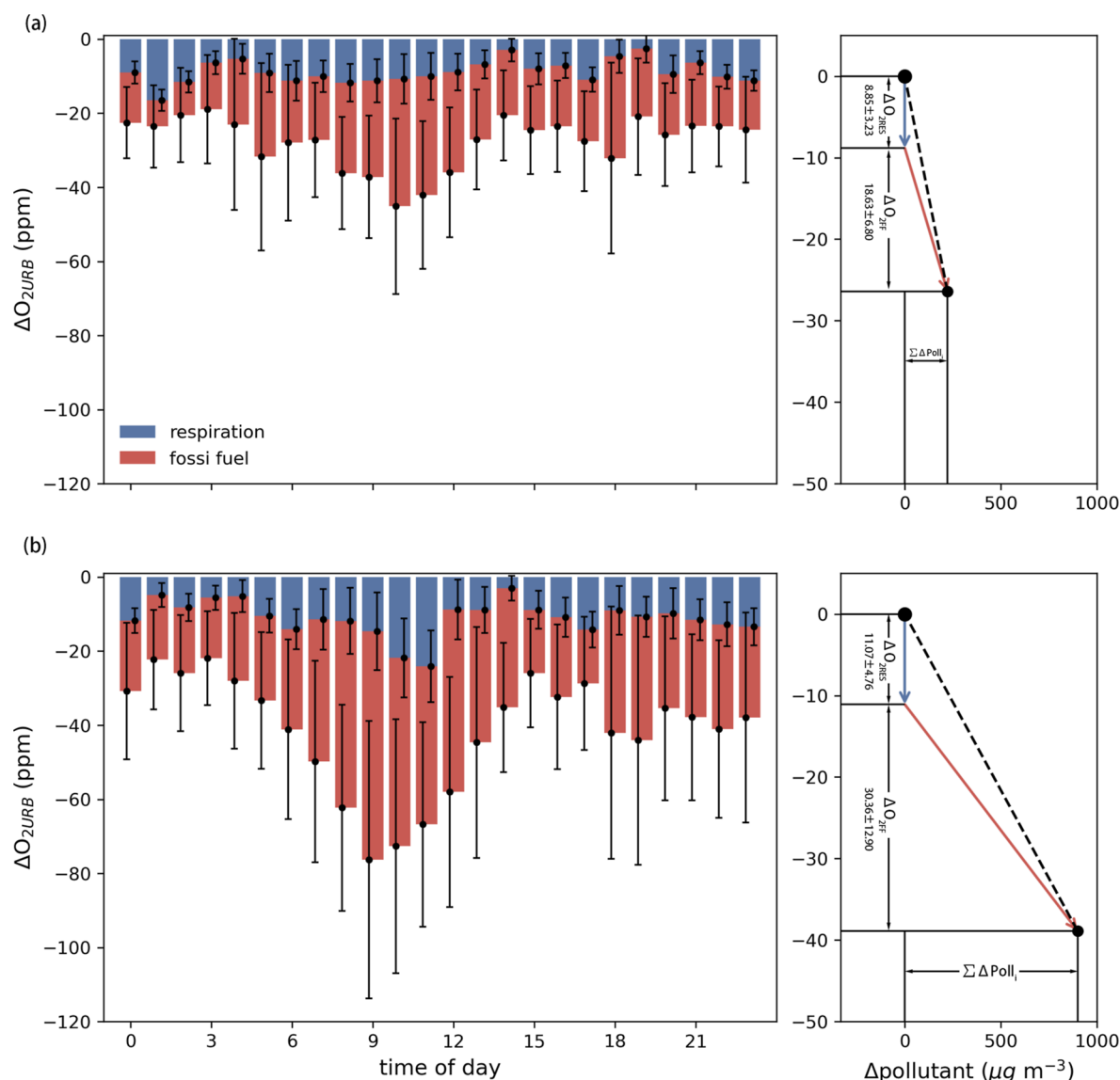


Figure 3. Contribution from respiration (blue) and fossil fuel combustion (red) to averaged hourly ΔO_{2URB} in clean (a) and polluted days (b). The right panels show the averaged changes in ΔO_{2URB} (y-axis) and Δ pollutants (x-concentration). The vectors illustrate the contribution of human respiration (blue) and fossil fuel combustion (red) related to the changes in ΔO_{2URB} (vertical axis) and Δ pollutants.

for each of the 24 h in clean and polluted sets. When we estimated k_i , all the $\Delta Poll_i$ are converted to the same unit ($\mu g/m^3$) and applied baseline removal. k_i (coefficient) is reported in $ppm/(\mu g/m^3)$ and ΔO_{2RES} (intercept) is reported in ppm. We calculated $k_i \cdot \Delta Poll_i$ (ΔO_{2FF} component for each pollutant) using the observation and the derived coefficients from the bootstrap experiments to derive the contribution from each pollutant ($k_i \cdot \Delta Poll_i / \Delta O_{2FF}$, see Figures S10, S11, and 4).

It is worth noting that pollutant selection is critical since the linear combination of pollutant concentration is designed to reflect the intensity of fossil fuel combustion. If insufficient pollutants are selected for solving eq 5, ΔO_{2FF} is prone to be underfitted, leading to an overestimation of ΔO_{2RES} . Thus, optimal pollutant selections should be conducted. Here, we adopted recursive feature elimination (RFE) to select the most valuable combination of pollutants in the solution of eq 5. RFE is a widely used feature selection algorithm in machine learning models. The goal of RFE is to select valuable features by recursively considering smaller and smaller sets of features

(pollutants). First, the regressor is trained on the initial set of features (pollutants) and the importance of each feature (pollutant) is obtained through regression coefficients. Then, the least important features (pollutants) are pruned from the current set of features (pollutants). That procedure is recursively repeated on the pruned set until the desired number of features (pollutants) to select is eventually reached. To find the optimal number of features, we conducted 5000 bootstraps for RFE as the number of pollutants was specified from 1 to 9. The nine pollutants initially introduced are CO, NO, NO₂, SO₂, EC (elementary carbon in PM_{2.5}), OC (organic carbon in PM_{2.5}), PM₁, PM_{2.5}, and PM₁₀.

RESULTS

Urban Impact on O₂ and Pollutant Levels. The ΔO_2 in the urban region displayed strong daily and seasonal cycles. The highest ΔO_2 was observed in summer, while the lowest ΔO_2 was observed in winter (see Fig S3). Both natural and anthropogenic factors contribute to O₂ fluxes into and out of

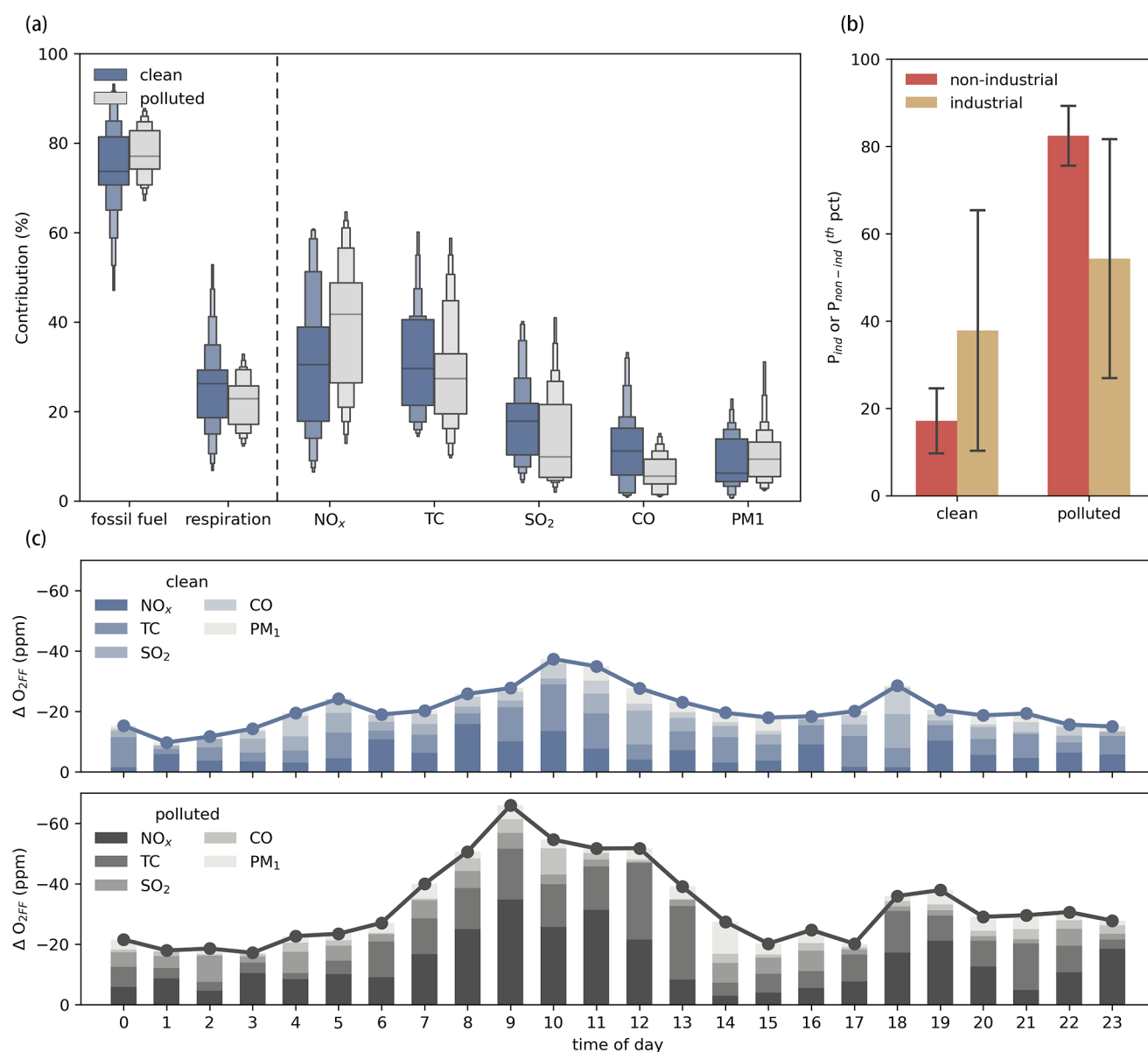


Figure 4. Contribution of potential pollutant sources to ΔO_2 . (a) Daily averaged contribution from fossil-fuel-related pollutants (NO_x , TC, SO_2 , CO, and PM_{10}) to ΔO_{2FF} on clean (blue) and polluted (grey) days. (b) Footprint percentile of industrial (orange) and nonindustrial (red) buildings under clean and polluted days. (c) Averaged diurnal cycle of ΔO_{2FF} on clean and polluted days.

the atmosphere, including variations in O_2 sources (photosynthesis) and sinks (anthropogenic O_2 consumption, etc.) and atmospheric stability that determines the dispersion and transport in the urban atmosphere. In summer, high O_2 content is mainly attributed to vegetation oxygen production and enhanced atmospheric mixing. In contrast, low ΔO_2 during winter is caused by frequent stagnant weather and surface inversion that inhibit pollutant dispersion, intensified O_2 consumption due to domestic heating, and a reduced photosynthetic effect. Due to sparse vegetation in both urban and natural landscapes in the semiarid region (Figure 1b), especially during winter, the influence of biological fluxes on ΔO_2 in Lanzhou is limited. Anthropogenic O_2 consumption and atmospheric stability seem to dominate ΔO_2 in downtown Lanzhou during the cold seasons, whereas in the warm seasons O_2 production via vegetation photosynthesis becomes apparent.

To highlight the urban impact on the anthropogenic O_2 and pollutant levels (ΔO_{2URB} and $\Delta Poll_i$), we divided the observations into two groups: clean days and polluted days based on P_{urb} , the metric to quantify the urban influence on the observation site (see Methods). The averaged footprint and $P_{urb}(x,y)$ for clean and polluted days are shown in Figs. S7 & S8. The averaged diurnal cycle and concentrations of ΔO_{2URB} under clean and polluted days are shown in Figure 2. The diurnal cycles of ΔO_{2URB} displayed two troughs near the morning and evening rush hours. Clean days feature higher ΔO_{2URB} , lower pollutant levels, and weaker diurnal cycle, while lower ΔO_{2URB} , higher pollutant levels, and amplified diurnal cycle are observed during polluted days. Pronounced antiphase patterns between O_2 and atmospheric pollutants are found on both clean and polluted days. High levels of O_2 are typically associated with low particulate and gaseous pollutants, implying good air quality, while declining O_2 content suggests deteriorating air quality. Robust anticorrelations between O_2

and gaseous oxides, including CO, NO_x, and SO₂, were observed throughout the year. The generation of these pollutants is associated with direct O₂ consumption as fossil fuel is combusted. Stronger $\Delta O_{2URB}-\Delta NO_x$ and $\Delta O_{2URB}-\Delta CO$ correlations than $\Delta O_{2URB}-\Delta SO_2$ indicate a larger contribution from transportation sectors to O₂ consumption in downtown Lanzhou,⁴¹ while enhanced O₂–SO₂ correlation during clean days may imply intracity transport of industrial pollutants.

For fine-particulate pollutants (PM_{2.5} and PM₁), stronger r_c (Pearson correlation coefficient) could be attributable to the increase in primary pollutants emitted as O₂ is consumed, while weaker r_p suggests enhanced secondary aerosol formation during the polluted episodes, which undermines the direct linkage between O₂ consumption and pollutant emissions. However, TC (EC and OC) in PM_{2.5}, which enters the atmosphere as both primary and secondary pollutants,⁴² is shown to correlate strongly with O₂ in polluted conditions. The contrast in $\Delta O_{2URB}-\Delta TC$ correlation between clean and polluted days implies a significant increase in both direct fossil-fuel-related O₂ consumption at ppm levels, and secondary formation of organic aerosol and inorganic aerosols at ppb levels as urban influence extends.

Breakdown of ΔO_{2URB} into Fossil Fuel Combustion and Human Respiration. In separating human respiration (ΔO_{2RES}) and fossil fuel combustion (ΔO_{2FF}) from the observed ΔO_{2URB} based on eq 5, the selection of pollutants is critical. Based on the RFE algorithm, optimal combinations of pollutants are picked as we gradually increase the number of pollutants introduced from 1 to 9. Figure S16a,b shows a significant improvement in fitting performance and declined ΔO_{2RES} as the number of pollutants increases. However, when more than seven pollutants are selected, no significant improvements in Pearson correlation were found and the downward trend of ΔO_{2RES} is halted. This demonstrates that the subsequent introduction of pollutants may lead to model redundancy and decrease explainability. Thus, the combination of the seven pollutants (CO, NO, NO₂, SO₂, EC, OC, and PM₁) can faithfully reproduce the O₂ decline due to fossil fuel combustion, whereas PM₁₀ and PM_{2.5} are excluded. The principal reason for the removal of PM_{2.5} and PM₁₀ is due to the relatively high contribution from both natural background emission and secondary formation in the absence of significant O₂ consumption^{35,37,43} (see Section S5 for details).

Figure 3 shows the diurnal cycle of ΔO_{2RES} and ΔO_{2FF} in Lanzhou on clean and polluted days. ΔO_{2RES} displays one trough in the morning, while ΔO_{2FF} displays two troughs during morning and evening rush hours in both clean and polluted days with comparable magnitude, contrasting a weaker evening trough of ΔO_{2URB} , particularly on clean days (Figure 2). There is little difference in local emission patterns in these two scenarios, as reflected in Figure 3. However, enhanced atmospheric dispersion on clean days brings nonfossil fuel influence from outer suburbs and thus offsets and weakens local signals. The diurnal cycle of ΔO_{2RES} is similar to the flux estimation by previous observational O₂–CO₂ studies,^{26,27} which is based on population statistics and assumed OR_{RES} of 1.2. Human respiration (ΔO_{2RES}) causes an 8.52 ± 3.23 ppm decline in O₂ during clean days and an 11.07 ± 4.76 ppm decline on polluted days. However, compared with clean days, $-\Delta O_{2FF}$ increased significantly from 18.63 ± 6.80 ppm (clean) to 30.36 ± 12.90 ppm (polluted). Both ΔO_{2RES} and ΔO_{2FF} display strong diurnal cycles, with a high contribution to O₂ decline during the daytime. Though both

$-\Delta O_{2RES}$ and $-\Delta O_{2FF}$ increase under polluted conditions, the drops in ΔO_{2URB} are mainly attributable to fossil fuel combustion. To further determine the fossil fuel impacts of each subsector on ΔO_{2URB} and air quality warrants further breakdown of ΔO_{2FF} and explorations on the varying relationships between ΔO_{2URB} and each pollutant under different conditions.

Intracity Atmospheric Transport Revealed by Tracing ΔO_{2FF} . Figure 4a shows the averaged contribution from ΔO_{2RES} and ΔO_{2FF} to ΔO_{2URB} . During clean days, 33.08% of the ΔO_{2URB} are due to ΔO_{2RES} and 66.92% due to ΔO_{2FF} , while during polluted days, ΔO_{2RES} only account for 27.50% of the ΔO_{2URB} , and 72.50% of the ΔO_{2URB} are attributable to ΔO_{2FF} . We further attributed ΔO_{2FF} to each fossil-fuel-related pollutant (see Methods). NO_x takes the largest share of ΔO_{2FF} in both clean and polluted days, followed by TC, SO₂, CO, and PM₁. Though higher ΔO_{2URB} levels and better air quality are observed during clean days, the potential contribution from various urban sources under clean and polluted conditions differs from each other. The O₂ variation under polluted days seems to be more affected by O₂ consumption processes linked to NO_x and PM₁ emissions. For clean days, however, the influence of SO₂ and CO has grown (Figure 4b).

Weather dynamics and large-scale atmospheric motions play essential roles in determining the source and extent of atmospheric pollution.⁴⁴ There are wide discrepancies in the vertical profiles of clean and polluted days (Figure S6). For clean days, the vertical profile featured updrafts near Lanzhou and cold anomalies in the lower troposphere. The updraft around Lanzhou indicated good atmospheric ventilation, which is conducive to the dispersion and transport of pollutants and air mass. On polluted days, the vertical profile was almost the opposite of the clean days, with warm anomalies and downdrafts on the near surface. Atmospheric sounding showed surface inversion below 750 hPa (only about 600 m above the ground), which prevents vertical dispersion of pollutants and exchange of fresh clean air, traps anthropogenic pollutants in the near surface, and results in declines in atmospheric O₂ levels.

Large-scale circulation provides essential context for the transport of air pollutants at the subcity scale. Under cleaner conditions, exchanges of air between the urban region and natural background are enhanced, while it also facilitates air exchanges at smaller spatiotemporal scales between the downtown and industrial zone. The STILT simulation further indicates a higher degree of industrial influence (denoted by percentile of P_{ind}) under cleaner conditions (see Section S3.1 and Figure S8) when enhanced atmospheric dilution supports long-range transport of air mass and pollutants and diminishes pollutants from local sources. In this study, the O₂ and pollutants were measured in the downtown (nonindustrial) region, which is about 22 km away from the heavy industrial regions. Therefore, during clean days, ΔO_{2URB} variations are attributable to be influenced by both industrial and non-industrial sectors. On polluted days, local nonindustrial sectors (transportation) dominate ΔO_{2URB} concentration due to suppressed atmospheric mixing. The attribution of the diurnal cycle shows two significant peaks in NO_x-related ΔO_{2FF} during rush hours, particularly for polluted days (Figure 4c), suggesting a high contribution from traffic-related fossil fuel combustion in the downtown region. According to the MEIC inventory⁴⁵ and a recently established anthropogenic emission

inventory for Lanzhou,⁴⁶ transportation is also the largest emission source of NO_x . For clean days, weaker oscillation of the diurnal cycle and fairly even shares from different pollutant sources manifest mixed O_2 consumption from both local and remote pollutant sources. The comparisons above highlight the role of intracity atmospheric transport under a well-mixed urban atmosphere and reveal the primary O_2 consumption sector (transportation) during polluted conditions.

DISCUSSION

By integrating the findings, we propose a conceptual scheme illustrating the critical air pollution and urban O_2 consumption processes during clean and polluted days in Figure 5. The

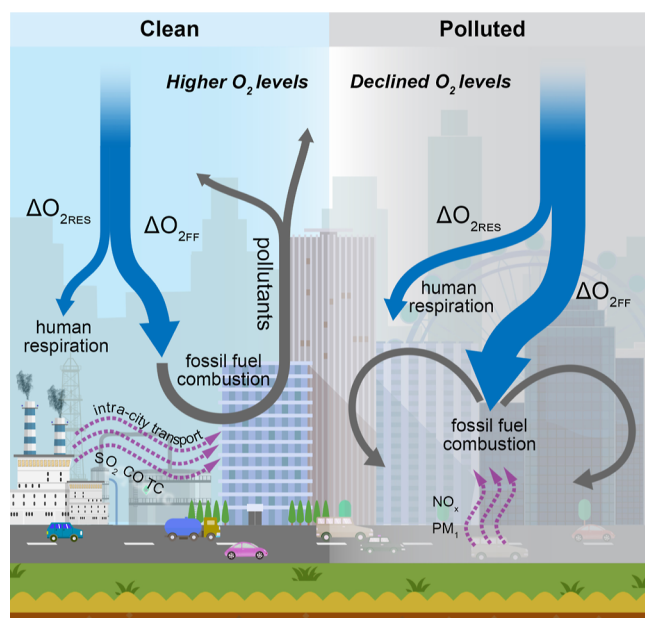


Figure 5. Conceptual scheme illustrating the critical air pollution processes during clean and polluted days. The blue arrows denote the “urban respiration” (human respiration and fossil fuel combustion). The grey arrows represent the pollutants emitted as fossil fuel is combusted, and the purple arrows indicate the intracity transport of pollutants from industrial sources (clean days) and emission enhancements from local sources (polluted days).

urban region “breathes in” atmospheric O_2 and “breath out” pollutants. Human respiration (33.08 and 27.50% for clean and polluted days, respectively) and fossil fuel combustion (66.92 and 72.50% for clean and polluted days, respectively) are major urban O_2 sinks in Lanzhou. On clean days, despite higher O_2 levels and improved air quality, good atmospheric mixing favors both diffusion and intracity transport of pollutants (SO_2 , CO , and TC) from industrial sources. On polluted days, with declining atmospheric O_2 and rising pollutant levels, inhibited atmospheric dispersion traps the local pollutants within the boundary layer, and nonindustrial emissions from local sources (transportation sectors) serve as the largest O_2 sink.

The neglect of human respiration can cause underestimations of emission ratios (ER, e.g., $\Delta\text{CO}/\Delta\text{CO}_2$ and $\Delta\text{NO}_x/\Delta\text{CO}_2$) derived from direct measurements since the observed CO_2 is misattributed to fossil fuel emissions. A lot of open-air observational studies impute the higher inventory-derived ER to overestimation by emission inventories,^{29,30,47} while excellent agreements between local inventory CO/CO_2 ratio for the traffic sector and the observed $\Delta\text{CO}/\Delta\text{CO}_2$ ratio

are obtained in a tunnel study, in which CO_2 and pollutants (CO , NO_x , and VOCs) measurements were performed in a road tunnel in Paris,⁴⁸ which is close to the origin of the air mass. It is worth stressing that the neglect of human respiration may not necessarily indicate that ERs from previous observations are incorrect, and bias may also occur in ERs derived from inventory. The observed ERs in the Paris study,⁴⁸ which is conducted in a tunnel close to the major emission sources, may be less influenced by human respiration. To mitigate the impact of human respiration on the observed ERs, we suggest that necessary adjustments are needed in the selection of observatory location (e.g., away from densely populated regions) and/or postprocessing of the observed CO_2 (e.g., subtraction of respiration-related component from the observed CO_2 variability). In addition, accurate estimation of the CO_2 and O_2 fluxes due to human respiration, especially for densely populated regions, could be important for constraining urban carbon budgets and the establishment of regional emission inventories.

The varying relationships between O_2 and pollutants under different conditions unfold the dynamics of urban respiration and provide insights into the anthropogenic O_2 and energy consumption, pollutant emission, and intracity atmospheric transport processes. This study is one of the first to break down urban O_2 variability based on simultaneous O_2 and pollutant measurements. It is worth noting that the conclusion should be interpreted with caution due to the following limitations of the study. Although an optimal combination of pollutants determined by the RFE algorithm is introduced to the linear model and variance inflation factor analysis has revealed a weak impact from multicollinearity (see Figure S20), the framework proposed in this study may not be able to fully capture the complex chemical transformations in the urban atmosphere (i.e., secondary generation of organic and inorganic aerosols including nitrate, sulfate, and ammonium). In addition, despite the removal of the baseline determined by the 99th (and 1st) percentile, the impact of biological flux on $\Delta\text{O}_{2\text{URB}}$ is not yet quantified. By inspecting the simulation bias, we found a larger negative bias (~ 1 ppm) in the afternoon and summertime when an enhanced effect of photosynthesis is observed (see Section S4.3). Nevertheless, it should be noted that the model bias could also be caused by other unknown sources. The lack of consideration for vegetation could be a potential bias that deserves further consideration for future studies.

Simultaneous measurements of O_2 , CO_2 , and fossil-fuel-related atmospheric pollutants are necessary. They can constrain the ORs for human respiration and fossil fuel combustion, providing additional constraints for regional and global carbon budgets as well as multiscale emission inventories. A similar research framework could be applied to a wider spatial domain to trace anthropogenic emission, energy, and O_2 consumption as well as calibrate emission inventories using multiple sources of observations including satellite retrievals,⁴⁹ urban mobile observations,^{50,51} and so forth. In addition, the nonlinear relationships among O_2 , CO_2 , and species with short lifetimes could be explored using nonlinear models, for example, the AI models including random forests regressor, deep neural networks, and so forth.

■ ASSOCIATED CONTENT

SI Supporting Information

The Supporting Information is available free of charge at <https://pubs.acs.org/doi/10.1021/acs.est.2c07583>.

Pollution measurements at the LACMS station; instrument bias correction for O₂ measurements; classification of clean and polluted days; background signal removal; and critical pollutants selection for ΔO_{2URB} breakdown (PDF)

■ AUTHOR INFORMATION

Corresponding Author

Jianping Huang – Collaborative Innovation Center for Western Ecological Safety, Lanzhou University, Lanzhou 730000, China; Land-atmosphere Interaction and Its Climatic Effects Group, State Key Laboratory of Tibetan Plateau Earth System, Resources and Environment (TPESRE), Institute of Tibetan Plateau Research, Beijing 100101, China; orcid.org/0000-0003-2845-797X; Email: hjp@lzu.edu.cn

Authors

Xiaoyue Liu – Key Laboratory for Semi-Arid Climate Change of the Ministry of Education, College of Atmospheric Sciences, Lanzhou University, Lanzhou 730000, China; orcid.org/0000-0001-8074-3362

Li Wang – Collaborative Innovation Center for Western Ecological Safety, Lanzhou University, Lanzhou 730000, China

Xinbo Lian – Key Laboratory for Semi-Arid Climate Change of the Ministry of Education, College of Atmospheric Sciences, Lanzhou University, Lanzhou 730000, China

Changyu Li – Key Laboratory for Semi-Arid Climate Change of the Ministry of Education, College of Atmospheric Sciences, Lanzhou University, Lanzhou 730000, China

Lei Ding – Key Laboratory for Semi-Arid Climate Change of the Ministry of Education, College of Atmospheric Sciences, Lanzhou University, Lanzhou 730000, China

Yun Wei – Department of Atmospheric Science, School of Environmental Studies, China University of Geosciences, Wuhan 430074, China

Siyu Chen – Key Laboratory for Semi-Arid Climate Change of the Ministry of Education, College of Atmospheric Sciences, Lanzhou University, Lanzhou 730000, China; orcid.org/0000-0003-2532-6050

Yongqi Wang – Key Laboratory for Semi-Arid Climate Change of the Ministry of Education, College of Atmospheric Sciences, Lanzhou University, Lanzhou 730000, China

Shixue Li – Graduate School of Environmental Science, Hokkaido University, Sapporo 060-0810, Japan

Jinsen Shi – Collaborative Innovation Center for Western Ecological Safety, Lanzhou University, Lanzhou 730000, China

Complete contact information is available at: <https://pubs.acs.org/doi/10.1021/acs.est.2c07583>

Author Contributions

X.L. and J.H. designed the study and contributed to the ideas, data analysis, and manuscript writing. L.W. and X.L. contributed to the data processing, interpretation, and manuscript writing. All of the authors contributed to the

discussion and interpretation of the manuscript. All of the authors reviewed the manuscript.

Notes

The authors declare no competing financial interest.

■ ACKNOWLEDGMENTS

This work was jointly supported by the National Science Foundation of China (41991231 and 91937302), the Second Tibetan Plateau Scientific Expedition and Research Program (STEP), grant no. 2019QZKK0602, the Youth Science and Technology Fund Project of Gansu Province of China (21JR7RA528), and the Fundamental Research Funds for the Central Universities (lzujbky-2021-64).

■ REFERENCES

- (1) United Nations Population Division. World Urbanization Prospects: The 2018 Revision, 2018. <https://population.un.org/wup/Publications/Files/WUP2018-Report.pdf> (accessed Dec 25, 2022).
- (2) Churkina, G. The Role of Urbanization in the Global Carbon Cycle. *Front. Ecol. Evol.* **2016**, 3. DOI: 10.3389/fevo.2015.00144.
- (3) Wang, J.; Feng, J.; Yan, Z.; Chen, Y. Future Risks of Unprecedented Compound Heat Waves Over Three Vast Urban Agglomerations in China. *Earth's Future* **2020**, 8, No. e2020EF001716.
- (4) Huang, J.; Li, Y.; Fu, C.; Chen, F.; Fu, Q.; Dai, A.; Shinoda, M.; Ma, Z.; Guo, W.; Li, Z.; Zhang, L.; Liu, Y.; Yu, H.; He, Y.; Xie, Y.; Guan, X.; Ji, M.; Lin, L.; Wang, S.; Yan, H.; Wang, G. Dryland Climate Change: Recent Progress and Challenges. *Rev. Geophys.* **2017**, 55, 719–778.
- (5) Liang, D.; Shi, L.; Zhao, J.; Liu, P.; Sarnat, J. A.; Gao, S.; Schwartz, J.; Liu, Y.; Ebelt, S. T.; Scovronick, N.; Chang, H. H. Urban Air Pollution May Enhance COVID-19 Case-Fatality and Mortality Rates in the United States. *Innovation* **2020**, 1, 100047.
- (6) Guo, W.; Chen, B.; Li, G.; Liu, M.; Liu, X.; Chen, Q.; Zhang, X.; Li, S.; Chen, S.; Feng, W.; Zhang, R.; Chen, M.; Shi, T. Ambient PM_{2.5} and Related Health Impacts of Spontaneous Combustion of Coal and Coal Gangue. *Environ. Sci. Technol.* **2021**, 55, 5763–5771.
- (7) Chen, S.; Zhang, X.; Lin, J.; Huang, J.; Zhao, D.; Yuan, T.; Huang, K.; Luo, Y.; Jia, Z.; Zang, Z.; Qiu, Y.; Xie, L. Fugitive Road Dust PM_{2.5} Emissions and Their Potential Health Impacts. *Environ. Sci. Technol.* **2019**, 53, 8455–8465.
- (8) Wei, Y.; Wu, J.; Huang, J.; Liu, X.; Han, D.; An, L.; Yu, H.; Huang, J. Declining Oxygen Level as an Emerging Concern to Global Cities. *Environ. Sci. Technol.* **2021**, 55, 7808–7817.
- (9) Li, C.; Huang, J.; Ding, L.; Liu, X.; Yu, H.; Huang, J. Increasing Escape of Oxygen From Oceans Under Climate Change. *Geophys. Res. Lett.* **2020**, 47, No. e2019GL086345.
- (10) Huang, J.; Liu, X.; He, Y.; Shen, S.; Hou, Z.; Li, S.; Li, C.; Yao, L.; Huang, J. The Oxygen Cycle and a Habitable Earth. *Sci. China Earth Sci.* **2021**, 64, 511–528.
- (11) Liu, X.; Huang, J.; Huang, J.; Li, C.; Ding, L.; Meng, W. Estimation of Gridded Atmospheric Oxygen Consumption from 1975 to 2018. *J. Meteorol. Res.* **2020**, 34, 646–658.
- (12) Keeling, R. F.; Manning, A. C. *Studies of Recent Changes in Atmospheric O₂ Content*, 2nd ed.; Elsevier Ltd., 2014; Vol. 5. DOI: 10.1016/B978-0-08-095975-7.00420-4.
- (13) Keeling, R. F. *Development of an Interferometric Oxygen Analyzer for Precise Measurement of the Atmospheric O₂ Mole Fraction*; Harvard University: Cambridge, 1988.
- (14) Huang, J.; Huang, J.; Liu, X.; Li, C.; Ding, L.; Yu, H. The Global Oxygen Budget and Its Future Projection. *Sci. Bull.* **2018**, 63, 1180–1186.
- (15) Han, D.; Huang, J.; Ding, L.; Liu, X.; Li, C.; Yang, F. Oxygen Footprint: An Indicator of the Anthropogenic Ecosystem Changes. *Catena* **2021**, 206, 105501.

- (16) Han, D.; Huang, J.; Ding, L.; Zhang, G.; Liu, X.; Li, C.; Yang, F. Breaking the Ecosystem Balance Over the Tibetan Plateau. *Earth's Future* **2022**, *10*, No. e2022EF002890.
- (17) Yan, Y.; Brook, E. J.; Kurbatov, A. v.; Severinghaus, J. P.; Higgins, J. A. Ice Core Evidence for Atmospheric Oxygen Decline since the Mid-Pleistocene Transition. *Sci. Adv.* **2021**, *7*, No. eabj9341.
- (18) Shi, P.; Chen, Y.; Zhang, G.; Tang, H.; Chen, Z.; Yu, D.; Yang, J.; Ye, T.; Wang, J.; Liang, S.; Ma, Y.; Wu, J.; Gong, P. Factors contributing to spatial-temporal variations of observed oxygen concentration over the Qinghai-Tibetan Plateau. *Sci. Rep.* **2021**, *11*, 17338.
- (19) Chen, Y.; Zhang, G.; Chen, Z.; Yang, X.; Chen, B.; Ma, Y.; Xie, H.; Luo, Q.; Yang, J.; Ye, T.; Yu, D.; Wang, J.; Tang, H.; Chen, Z.; Shi, P. A Warming Climate May Reduce Health Risks of Hypoxia on the Qinghai-Tibet Plateau. *Sci. Bull.* **2022**, *67*, 341–344.
- (20) Cai, Q.; Zeng, N.; Zhao, F.; Han, P.; Liu, D.; Lin, X.; Chen, J. The Impact of Human and Livestock Respiration on CO₂ Emissions from 14 Global Cities. *Carbon Bal. Manag.* **2022**, *17*, 11–12.
- (21) Klein Goldewijk, K. K.; Beusen, A.; Doelman, J.; Stehfest, E. Anthropogenic Land Use Estimates for the Holocene - HYDE 3.2. *Earth Syst. Sci. Data* **2017**, *9*, 927–953.
- (22) Ciais, P.; Bousquet, P.; Freibauer, A.; Naegler, T. Horizontal Displacement of Carbon Associated with Agriculture and Its Impacts on Atmospheric CO₂. *Global Biogeochem. Cycles* **2007**, *21*, a.
- (23) Moriwaki, R.; Kanda, M. Seasonal and Diurnal Fluxes of Radiation, Heat, Water Vapor, and Carbon Dioxide over a Suburban Area. *J. Appl. Meteorol. Climatol.* **2004**, *43*, 1700–1710.
- (24) Goret, M.; Masson, V.; Schoetter, R.; Moine, M. P. Inclusion of CO₂ Flux Modelling in an Urban Canopy Layer Model and an Evaluation over an Old European City Centre. *Atmos. Environ.: X* **2019**, *3*, 100042.
- (25) Cai, Q.; Yan, X.; Li, Y.; Wang, L. Global Patterns of Human and Livestock Respiration. *Sci. Rep.* **2018**, *8*, 3–6.
- (26) Ishidoya, S.; Sugawara, H.; Terao, Y.; Kaneyasu, N.; Aoki, N.; Tsuboi, K.; Kondo, H. L. O₂ : CO₂ exchange ratio for net turbulent flux observed in an urban area of Tokyo, Japan, and its application to an evaluation of anthropogenic CO₂ emissions. *Atmos. Chem. Phys.* **2020**, *20*, 5293–5308.
- (27) Sugawara, H.; Ishidoya, S.; Terao, Y.; Takane, Y.; Kikigawa, Y.; Nakajima, K. Anthropogenic CO₂ Emissions Changes in an Urban Area of Tokyo, Japan, Due to the COVID-19 Pandemic: A Case Study During the State of Emergency in April-May 2020. *Geophys. Res. Lett.* **2021**, *48*, 1–10.
- (28) Steinbach, J.; Gerbig, C.; Rödenbeck, C.; Karstens, U.; Minejima, C.; Mukai, H.; Rödenbeck, C.; Karstens, U.; Minejima, C.; Mukai, H. The CO₂ release and Oxygen uptake from Fossil Fuel Emission Estimate (COFFEE) dataset: effects from varying oxidative ratios. *Atmos. Chem. Phys.* **2011**, *11*, 6855–6870.
- (29) Wu, D.; Liu, J.; Wennberg, P. O.; Palmer, P. I.; Nelson, R. R.; Kiel, M.; Eldering, A. Towards Sector-Based Attribution Using Intracity Variations in Satellite-Based Emission Ratios between CO₂ and CO. *Atmos. Chem. Phys.* **2022**, *22*, 14547–14570.
- (30) Bares, R.; Lin, J. C.; Hoch, S. W.; Baasandorj, M.; Mendoza, D. L.; Fasoli, B.; Mitchell, L.; Catharine, D.; Stephens, B. B. The Wintertime Covariation of CO₂ and Criteria Pollutants in an Urban Valley of the Western United States. *J. Geophys. Res.: Atmos.* **2018**, *123*, 2684–2703.
- (31) Wu, D.; Lin, J.; Fasoli, B.; Oda, T.; Ye, X.; Lauvaux, T.; Yang, E.; Kort, E. A Lagrangian approach towards extracting signals of urban CO₂ emissions from satellite observations of atmospheric column CO₂ (XCO₂): X-Stochastic Time-Inverted Lagrangian Transport model ("X-STILT v1"). *Geosci. Model Dev.* **2018**, *11*, 4843–4871.
- (32) Fasoli, B.; Lin, J. C.; Bowling, D. R.; Mitchell, L.; Mendoza, D. Simulating atmospheric tracer concentrations for spatially distributed receptors: updates to the Stochastic Time-Inverted Lagrangian Transport model's R interface (STILT-R version 2). *Geosci. Model Dev.* **2018**, *11*, 2813–2824.
- (33) Ching, J.; Mills, G.; Bechtel, B.; See, L.; Feddema, J.; Wang, X.; Ren, C.; Brousse, O.; Martilli, A.; Neophytou, M.; Mouzourides, P.; Stewart, I.; Hanna, A.; Ng, E.; Foley, M.; Alexander, P.; Aliaga, D.; Niyogi, D.; Shreevastava, A.; Bhalachandran, P.; Masson, V.; Hidalgo, J.; Fung, J.; Andrade, M.; Baklanov, A.; Dai, W.; Milcinski, G.; Demuzere, M.; Brunsell, N.; Pesaresi, M.; Miao, S.; Mu, Q.; Chen, F.; Theeuwes, N. WUDAPT: An Urban Weather, Climate, and Environmental Modeling Infrastructure for the Anthropocene. *Bull. Am. Meteorol. Soc.* **2018**, *99*, 1907–1924.
- (34) World Health Organization (WHO). Air quality database: Update, 2011. <https://www.who.int/data/gho/data/themes/air-pollution/who-air-quality-database/2011> (accessed Dec 25, 2022).
- (35) Du, T.; Wang, M.; Guan, X.; Zhang, M.; Zeng, H.; Chang, Y.; Zhang, L.; Tian, P.; Shi, J.; Tang, C. Characteristics and Formation Mechanisms of Winter Particulate Pollution in Lanzhou, Northwest China. *J. Geophys. Res.: Atmos.* **2020**, *125*, 1–17.
- (36) Lanzhou Municipal Bureau of Statistics; Lanzhou Investigation Team (National Bureau of Statistics). *Lanzhou Statistical Yearbook 2020*; China Statistics Press, 2020.
- (37) Wang, M.; Tian, P.; Wang, L.; Yu, Z.; Du, T.; Chen, Q.; Guan, X.; Guo, Y.; Zhang, M.; Tang, C.; Chang, Y.; Shi, J.; Liang, J.; Cao, X.; Zhang, L. High contribution of vehicle emissions to fine particulate pollutions in Lanzhou, Northwest China based on high-resolution online data source appointment. *Sci. Total Environ.* **2021**, *798*, 149310.
- (38) Steinbach, J. *Enhancing the Usability of Atmospheric Oxygen Measurements through Emission Source Characterization and Airborne Measurements*; Friedrich Schiller University, 2010.
- (39) Berhanu, T. A.; Hoffnagle, J.; Rella, C.; Kimhak, D.; Nyfeler, P.; Leuenberger, M. High-Precision Atmospheric Oxygen Measurement Comparisons between a Newly Built CRDS Analyzer and Existing Measurement Techniques. *Atmos. Meas. Tech.* **2019**, *12*, 6803–6826.
- (40) Lin, J. C. A. A near-field tool for simulating the upstream influence of atmospheric observations: The Stochastic Time-Inverted Lagrangian Transport (STILT) model. *J. Geophys. Res.* **2003**, *108*, ACH 2-1–ACH 2-17, DOI: 10.1029/2002JD003161.
- (41) Reşitoğlu, İ. A.; Altinişik, K.; Keskin, A. The Pollutant Emissions from Diesel-Engine Vehicles and Exhaust Aftertreatment Systems. *Clean Technol. Environ. Policy* **2015**, *17*, 15–27.
- (42) Szidat, S.; Ruff, M.; Perron, N.; Wacker, L.; Synal, H.-A.; Hallquist, M.; Shannigrahi, A. S.; Yttri, K. E.; Dye, C.; Simpson, D. Fossil and non-fossil sources of organic carbon (OC) and elemental carbon (EC) in Göteborg, Sweden. *Atmos. Chem. Phys.* **2009**, *9*, 1521–1535.
- (43) Guan, X.; Wang, M.; Du, T.; Tian, P.; Zhang, N.; Shi, J.; Chang, Y.; Zhang, L.; Zhang, M.; Song, X.; Sun, Y. Wintertime Aerosol Optical Properties in Lanzhou, Northwest China: Emphasis on the Rapid Increase of Aerosol Absorption under High Particulate Pollution. *Atmos. Environ.* **2021**, *246*, 118081.
- (44) Cai, W.; Li, K.; Liao, H.; Wang, H.; Wu, L. Weather Conditions Conducive to Beijing Severe Haze More Frequent under Climate Change. *Nat. Clim. Change* **2017**, *7*, 257–262.
- (45) Li, M.; Liu, H.; Geng, G.; Hong, C.; Liu, F.; Song, Y.; Tong, D.; Zheng, B.; Cui, H.; Man, H.; Zhang, Q.; He, K. Anthropogenic Emission Inventories in China: A Review. *Natl. Sci. Rev.* **2017**, *4*, 834–866.
- (46) Guo, W.; Li, G.; Chen, B.; Xia, J.; Zhang, R.; Liu, X.; Zhu, Y.; Chen, Q. Establishment of a High-Resolution Anthropogenic Emission Inventory and Its Evaluation Using the WRF-Chem Model for Lanzhou. *Environ. Sci.* **2021**, *42*, 634–642.
- (47) Che, K.; Liu, Y.; Cai, Z.; Yang, D.; Wang, H.; Ji, D.; Yang, Y.; Wang, P. Characterization of Regional Combustion Efficiency using ΔXCO₂: ΔXCO₂ Observed by a Portable Fourier-Transform Spectrometer at an Urban Site in Beijing. *Adv. Atmos. Sci.* **2022**, *39*, 1299–1315.
- (48) Ammoura, L.; Xueref-Remy, I.; Gros, V.; Baudic, A.; Bonsang, B.; Petit, J.-E.; Perrussel, O.; Bonnaire, N.; Sciare, J.; Chevallier, F. Atmospheric measurements of ratios between CO₂ and co-emitted species from traffic: a tunnel study in the Paris megacity. *Atmos. Chem. Phys.* **2014**, *14*, 12871–12882.

(49) Reuter, M.; Buchwitz, M.; Hilboll, A.; Richter, A.; Schneising, O.; Hilker, M.; Heymann, J.; Bovensmann, H.; Burrows, J. P. Decreasing Emissions of NO_x Relative to CO₂ in East Asia Inferred from Satellite Observations. *Nat. Geosci.* **2014**, *7*, 792–795.

(50) Mitchell, L. E.; Crosman, E. T.; Jacques, A. A.; Fasoli, B.; Leclair-Marzolf, L.; Horel, J.; Bowling, D. R.; Ehleringer, J. R.; Lin, J. C. Monitoring of Greenhouse Gases and Pollutants across an Urban Area Using a Light-Rail Public Transit Platform. *Atmos. Environ.* **2018**, *187*, 9–23.

(51) Mallia, D. v.; Mitchell, L. E.; Kunik, L.; Fasoli, B.; Bares, R.; Gurney, K. R.; Mendoza, D. L.; Lin, J. C. Constraining Urban CO₂ Emissions Using Mobile Observations from a Light Rail Public Transit Platform. *Environ. Sci. Technol.* **2020**, *54*, 15613–15621.

Recommended by ACS

Mapping the Contribution of Biomass Burning to Persistent Organic Pollutants in the Air of the Indo-China Peninsula Based on a Passive Air Monitoring Network

Haoyu Jiang, Gan Zhang, *et al.*

JANUARY 19, 2023

ENVIRONMENTAL SCIENCE & TECHNOLOGY

[READ !\[\]\(4fe57c3593bf1b21d272ae7ac8dfaf77_img.jpg\)](#)

Correspondence on “Home is Where the Pipeline Ends: Characterization of Volatile Organic Compounds Present in Natural Gas at the Point of the Residential End User”

Misbath Daouda, Diana Hernández, *et al.*

JANUARY 19, 2023

ENVIRONMENTAL SCIENCE & TECHNOLOGY

[READ !\[\]\(b64b40baaee5acddc1eab8538ba84754_img.jpg\)](#)

Linking Life Cycle and Integrated Assessment Modeling to Evaluate Technologies in an Evolving System Context: A Power-to-Hydrogen Case Study for the United States

Patrick Lamers, Vassilis Daioglou, *et al.*

FEBRUARY 01, 2023

ENVIRONMENTAL SCIENCE & TECHNOLOGY

[READ !\[\]\(c15650232aa6660c9deb34f3b82dcb72_img.jpg\)](#)

Aging of Nanoplastics Significantly Affects Protein Corona Composition Thus Enhancing Macrophage Uptake

Tingting Du, Lijun Wu, *et al.*

FEBRUARY 02, 2023

ENVIRONMENTAL SCIENCE & TECHNOLOGY

[READ !\[\]\(2885535958616e9ec6b97903614c334b_img.jpg\)](#)

[Get More Suggestions >](#)